1 Preface

1.1 Context

This four-month USRA project was undertaken with the supervision of Professor Wayne Nagata and Professor Priscilla Greenwood. Here we investigated the stochastic Morris-Lecar neuron, comparing different models and measuring statistics such as interspike interval (ISI) distributions and exit times.

This report is a summary of the work the author has done, and serves as a companion to the codebase developed for this project. There are two types of readers this report targets: knowledgable researchers (such as Professor Priscilla and Professor Nagata) who can find results and code annotations handy in this report, and new students who would additionally benefit from the discussions of theory and resource recommendations.

1.2 Acknowledgements

I express my gratitude towards Professor Nagata and Professor Greenwood for introducing me to mathematical neuroscience, as well as engaging me more into nonlinear dynamics and stochastics. I have learned a lot from Professor Greenwood and Professor Nagata, and I thank them for supervising me.

I also thank the Natural Sciences and Engineering Research Council of Canada for helping fund this project with a USRA.

1.3 Contact Me

I can be reached out to by email (as of the time of this writing) at jwu277@gmail.com.

2 Code Usage

The code developed for this project can be found (as of the time of this writing) at `https://github.com/jwu277/usra2021`. The software is written in Python 3.

2.1 Code Structure

The project repoository is divided into three directories:

1. `neurons:` these files contain classes that are numerical implementations of various neuron models.
2. `scripts:` these files contain runnable scripts that perform various simulations.
3. `util:` these files contain various useful functions that files in the `neurons` and `scripts` directories may use.

Functions and variables starting with an underscore (e.g. `_a`) are intended to be used as private entities (i.e. only used within the file). Another thing is that each `neuron` file except for `neuron.mlr` has a corresponding `scripts` file with the same name that can be run for a quick simulation of the neuron. This mapping is not surjective, however. Now, some scripts will have a line similar to

```
    THREADS = 12
```

Feel free to change the number to the appropriate number of threads in your machine. Finally, scripts will sometimes have parameters such as `tmax`, `trials`, etc. As with most variables in the scripts, these can be changed to suit your needs.

A description of the files in the repository is given in **Table 2.1**. Of course, the code files themselves contain more detailed annotations.

File	Description	Notes
`neurons/bm.py`	Binary Markov (i.e. 2-state) neuron	
`neurons/izhikevich.py`	Izhikevich neuron	
`neurons/lif.py`	Linear integrate and fire neuron	
`neurons/ml.py`	Morris-Lecar neuron	

`neurons/mlj.py`	Jacobi Morris-Lecar neuron	Needs to be initialized with `init` before usage
`neurons/mll.py`	Linear Morris-Lecar neuron ($\tilde{\mathbf{x}}$)	Needs to be initialized with `init` before usage
`neurons/mlr.py`	Linear Distance Morris-Lecar neuron	Not really used. Simulates the modulus of the linear Morris-Lecar neuron.
`neurons/modelb.py`	"Model B" neuron; related to the patched model.	Patched model still needs to be investigated further, so work can still be done here.
`scripts/bm.py`	ISI distribution simulation for the binary Markov neuron	
`scripts/contour.py`	TODO	ipsum
`scripts/det.py`	Compares deterministic trajectories of different neuron models	
`scripts/docheck.py`	TODO	ipsum
`scripts/dtstab.py`	Compares different values of dt and numerical methods(currently Euler and RK45)	$dt = 0.1$ suffices. Also, no appreciable difference was observed between the Euler and RK45 methods.
`scripts/elstats.py`	TODO	ipsum
`scripts/isih.py`	TODO	ipsum
`scripts/izhikevich.py`	ISI distribution simulation for the Izhikevich neuron withPoisson current	Not really used and might have inconsistent units
`scripts/lif.py`	ISI distribution simulation for the LIF neuron	
`scripts/longtin.py`	Simulation of Longtin's stochastic bistable system	Simulation does not reproduce Longtin's results
`scripts/ml.py`	Simulation of a single trajectory of the Morris-Lecar neuron	

`scripts/mlj.py`	Simulation of a single trajectory of the Jacobi Morris-Lecar neuron	
`scripts/mll.py`	Simulation of a single trajectory of the linear Morris-Lecar neuron	
`scripts/mlrtrials.py`	TODO	ipsum
`scripts/modelb.py`	Simulation of a single trajectory of the Model B neuron	
`scripts/pdist.py`	TODO	ipsum
`scripts/phi_noise.py`	Saves a run of Morris-Lecar neuron for certain values ofϕ and N_K	Filename for save should be renamed as desired
`scripts/plotter.py`	Makes an animated plot of a phase portrait trajectory	Requires ImageMagick to be installed
`scripts/poincare.py`	TODO	ipsum
`scripts/sandbox.py`	Sandbox to play around in	
`util/current.py`	Generates $I(t)$ signal	
`util/dyn.py`	Used to find fixed point of a system	
`util/integrate.py`	Essentially a wrapper for `scipy.integrate.solve_ivp`	
`util/isi.py`	Computes spike times and ISIs in a signal	
`util/ito.py`	Euler-Maruyama method implementation	
`util/ml.py`	TODO	ipsum
`util/plot.py`	Handy plotting functions	

Table 2.1: *Descriptions of all the code files in the project repository.*

2.2 Running Scripts

First, a new user will likely need to run

```
python -m pip install -r requirements.txt
```

in a terminal at the root of the repository. Note: `python` is taken to be the alias for Python 3. After that, the dependencies should be installed and scripts can now be run. To do so, execute

```
python -m scripts.<scriptname>
```

in a terminal again at the root of the repository. Here `<scriptname>` is the name of the script file (excluding the `.py` suffix) to be run. For example, to run a simulation of ISIs for a binary Markov neuron, run

```
python -m scripts.bm
```

As of the writing of this report, a plot should appear after a bit of computation time (exit the plot to terminate the program).

3 Morris-Lecar Neuron

3.1 Circuit Model

The Morris-Lecar description [8] models a neuron as having a membrane potential v, defined to be the difference in voltage between the inside and outside of the neuron cell. Current flows through potassium and calcium channels in the membrane, labelled as I_K and I_{Ca}, respectively. There is also some current arising form other ions, which is collectively totalled as the leak current I_L. The combined potassium, calcium, and leak channels each have an effective conductance (or, taking reciprocals, resistance) and potential. Finally, the membrane has a capacitance C. **Figure 3.1** depicts a circuit for this model.

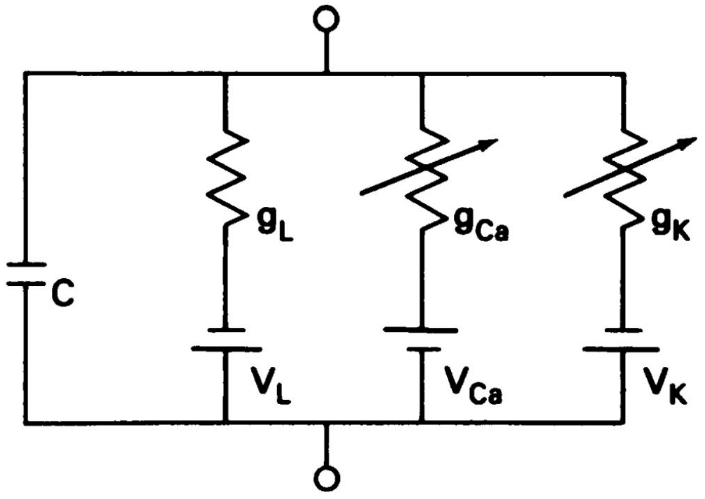

Figure 3.1: *Equivalent circuit of Morris-Lecar neuron model. Only g_{Ca} and g_K may vary with time–the other parameters in this diagram are constants. This diagram is copied from [8].*

Consequently, the membrane potential obeys the following first order differential equation:

$$C\frac{dv}{dt} = I - g_K(v - V_K) - g_{Ca}(v - V_{Ca}) - g_L(v - V_L) \tag{3.1}$$

Nominally, the potassium and calcium conductances are non-constant. Rather, they obey the following equations:

$$g_K = \bar{g}_K w \tag{3.2}$$
$$g_{Ca} = \bar{g}_{Ca} m \tag{3.3}$$

where $\bar{g}_K, \bar{g}_{Ca}$ are constant.

At constant v, the parameters $x = w, m$ are governed by first order differential equations of the following form:

$$\frac{dx}{dt} = \lambda_x(v)(x_\infty(v) - x) \tag{3.4}$$

However, the m timescale is much shorter than the w timescale, so that $m \approx m_\infty(v)$ in (3.1). Furthermore, to be consistent with [4], we may re-arrange the $x = w$ version of (3.4) to be of the following form:

$$\frac{dw}{dt} = \alpha(v)(1 - w) - \beta(v)w \tag{3.5}$$

Finally, we have

$$\alpha(v) = \frac{1}{2}\phi \cosh\left(\frac{v - V_3}{2V_4}\right)\left(1 + \tanh\left(\frac{v - V_3}{V_4}\right)\right) \tag{3.6}$$

$$\beta(v) = \frac{1}{2}\phi \cosh\left(\frac{v - V_3}{2V_4}\right)\left(1 - \tanh\left(\frac{v - V_3}{V_4}\right)\right) \tag{3.7}$$

$$m_\infty(v) = \frac{1}{2}\left(1 + \tanh\left(\frac{v - V_1}{V_2}\right)\right) \tag{3.8}$$

3.2 Morris-Lecar Parameters

The parameters from [4] used in this project are given in **Table 3.1**. Sometimes I and/or ϕ are varied to assess the bifurcational behaviuor of the system.

Variable	Value	Units
C	20	$\mu F/cm^2$
g_L	2.0	mS/cm^2
$\bar{g}_{Ca}$	4.4	mS/cm^2
$\bar{g}_K$	8	mS/cm^2
V_L	-60	mV
V_{Ca}	120	mV
V_K	-84	mV

Variable	Value	Units
V_1	-1.2	mV
V_2	18.0	mV
V_3	2.0	mV
V_4	30.0	mV
ϕ	0.04	ms^{-1}
I	90	$\mu A/cm^2$

Table 3.1: *Values of parameters used in the Morris-Lecar model. These values are assumed for the remainder of the report unless specified otherwise.*

3.3 Helpful Resources

The books [4] and [10] provide good introductions to the Morris-Lecar model.

4 Dynamics

4.1 Bautin Bifurcation

Consider a 2-dimensional dynamical system $(x(t), y(t)) \in \mathbb{R}^2$. We may equivalently define the complex variable $z = x + iy \in \mathbb{C}$. Alternatively, we may express this system in polar coordinates: $z = re^{i\varphi}$. Now, let us consider the system

$$\frac{dz}{dt} = \lambda z \left(1 + k_1 |z|^2 + k_2 |z|^4 + O\left(|z|^5\right)\right) \tag{4.1}$$
$$= \lambda z + c_1 z |z|^2 + c_2 z |z|^4 + O\left(|z|^6\right) \tag{4.2}$$

Here $c_j = \lambda k_j$, and $\lambda, c_j \in \mathbb{C}$ for $j = 1, 2$. Let us rewrite $\lambda = \alpha + i\omega, c_j = l_j + im_j$, where $\alpha, \omega, l_j, m_j \in \mathbb{R}$. Then taking real and imaginary parts of (4.2) gets us

$$\frac{dx}{dt} = (\alpha + l_1 r^2 + l_2 r^4)x - (\omega + m_1 r^2 + m_2 r^4)y \tag{4.3}$$
$$\frac{dy}{dt} = (\omega + m_1 r^2 + m_2 r^4)x + (\alpha + l_1 r^2 + l_2 r^4)y \tag{4.4}$$

Here we dropped terms of order $O\left(|z|^6\right)$ or higher. We do so by assuming that $l_2 < 0$ (and is thus nonzero). The parameter l_2, known as the *second Lyapunov coefficient*, is indeed negative for the Morris-Lecar neuron (as we shall discuss later). Doing some calculus, the equations for r and φ become:

$$\frac{dr}{dt} = r(\alpha + l_1 r^2 + l_2 r^4) \tag{4.5}$$
$$\frac{d\varphi}{dt} = \omega + m_1 r^2 + m_2 r^4 \tag{4.6}$$

We see that there is a fixed point at $r = 0$. Furthermore, there are circular limit cycles at r^2 satisfying the quadratic

$$f(r^2) = r^4 + \frac{l_1}{l_2} r^2 + \frac{\alpha}{l_2} = 0 \tag{4.7}$$

Since these limit cycles occur at $r > 0$, we have precisely one limit cycle for each r^2 root. The discriminant Δ of the quadratic (4.7) is

$$\Delta = \left(\frac{l_1}{l_2}\right)^2 - 4\frac{\alpha}{l_2} = \frac{1}{l_2^2}\left(l_1^2 - 4\alpha l_2\right) \tag{4.8}$$

The sign of Δ is therefore just the sign of $l_1^2 - 4\alpha l_2$. Then a necessary condition for there to be limit cycles i.e. positive real roots for r^2 is:

$$\alpha \geq \frac{l_1^2}{4l_2} \tag{4.9}$$

Now assuming that $\Delta \geq 0$ i.e. the roots for r^2 are all real, we use Vieta's formulas to note that the sum and product of the roots are $-\frac{l_1}{l_2}, \frac{\alpha}{l_2}$, repsectively.

For $\Delta \geq 0$, exactly one positive root exists precisely when $\alpha > 0 \therefore \frac{\alpha}{l_2} < 0$. But we immediately have $\alpha > 0 \geq \frac{l_1}{4l_2}$, satisfying the discriminant condition.

Now if $\alpha = 0$, then at least one root must coincide with $r = 0$. The other root is thus equal to $-\frac{l_1}{l_2}$ and is positive iff $l_1 > 0$.

Next, if $\alpha < 0$, both roots have the same sign. If $l_1 \leq 0$ then the sum of the roots is nonpositive, resulting in both roots being nonpositive. Thus there are no limit cycles for $\alpha < 0, l_1 \leq 0$. However, if $\alpha < 0$ and $l_1 > 0$, there are two positive roots for r^2 if $\alpha > \frac{l_1^2}{4l_2}$. If instead, $l_1 > 0$ and $\alpha = \frac{l_1^2}{4l_2} < 0$ then there is a repeated positive root and therefore one limit cycle.

Finally, the stability of the limit cycles and $r = 0$ fixed point is determined by the sign of $f(r^2)$ in between these roots. Since $l_2 < 0$, the outermost limit cycle (or fixed point if none exists) attracts from $r = \infty$. Meanwhile, the stability of the fixed point is determined by the sign of α (or l_1 if $\alpha = 0$, or $l_2 < 0$ if $\alpha, l_1 = 0$). Finally, if there are two limit cycles, the inner one is unstable while the outer one is stable since $f(r^2)$ is a downwards parabola in r^2.

Put all together, the bifurcation diagram is given in **Figure 4.1**

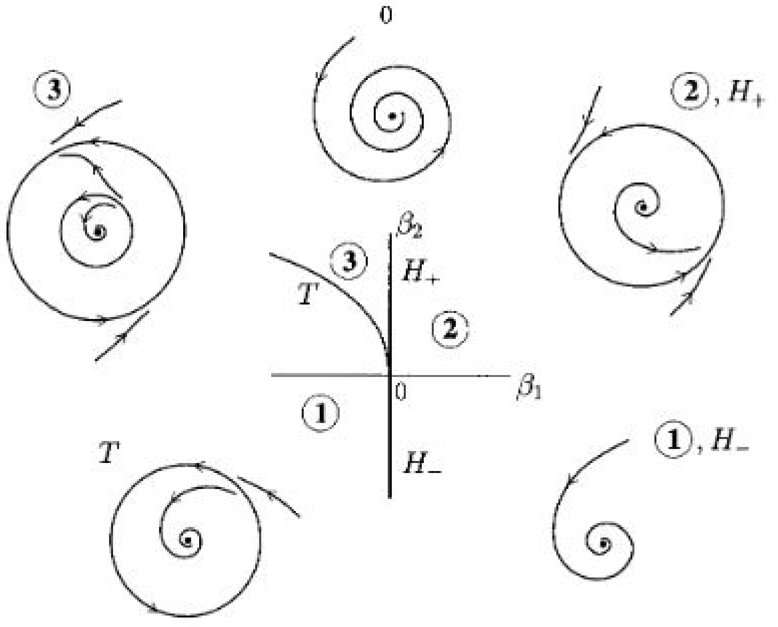

Figure 4.1: *Bifurcation diagram of Bautin bifurcation. This figure was obtained from [5]. This diagram labels α and l_1 as β_1 and β_2, respectively.*

The curve $H_- = \{\alpha = 0, l_1 < 0\}$, in **Figure 4.1** is a *Hopf bifurcation.* For a fixed $l_1 < 0$, varying α near zero affects the stability of the system; $\alpha < 0$ has a limit cycle whereas $\alpha > 0$ does not. Similarly, $H_+ = \{\alpha = 0, l_1 > 0\}$ is also a Hopf bifurcation. This time, a limit cycle is produced at the fixed point when varying $\alpha > 0$ to $\alpha < 0$. In general, the Hopf bifurcation is a local codim-1 bifurcation, where a limit cycle appears from/disappears into a fixed point.

The curve $T = \{l_1 > 0, \alpha = \frac{l_1^2}{4l_2}\}$ is a *saddle node of limit cycles (SNLC) bifurcation*. Here the two limit cycles in region 3 collapse into a single limit cycle on T. Varying a parameter more (e.g. decreasing α or l_1) will cause the semi-stable limit cycle to disappear. Like the Hopf bifurcation, the SNLC bifurcation is a local codim-1 bifurcation.

Finally, a *Bautin bifurcation* occurs near the point $\alpha, l_1 = 0$ in this model system. Since two parameters are varied in this bifurcation (α, l_1), this is a local codim-2 bifurcation.

4.2 Morris-Lecar Dynamics

A Bautin bifurcation exists for the Morris-Lecar neuron in the parameters (I, ϕ) near $(I, \phi) = (90, 0.04)$. The bifurcation diagram is given in **Figure 4.2**. We see that

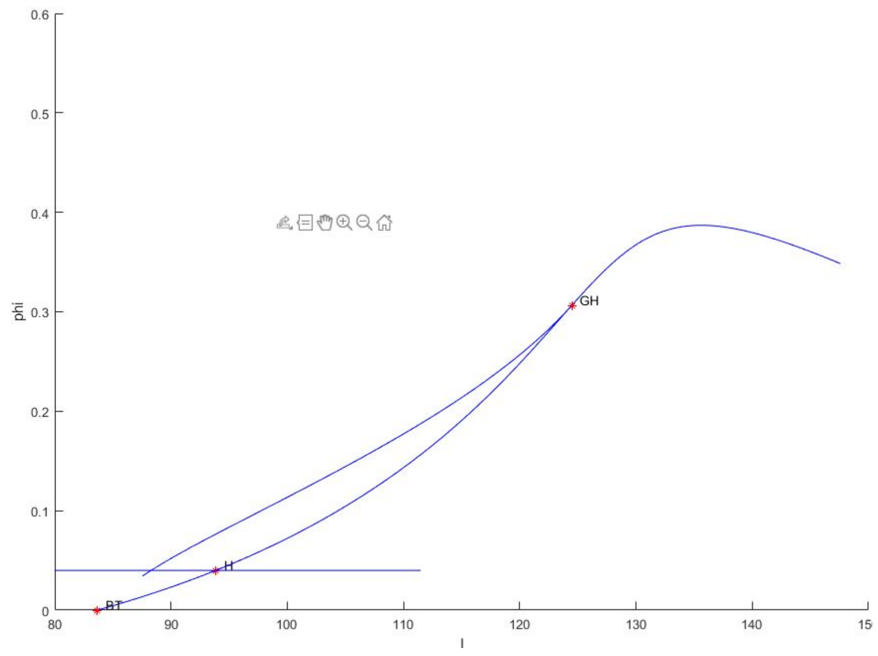

Figure 4.2: *TODO: get better image (maybe plot in python?)*

$(I, \phi) = (90, 0.04)$ corresponds to a system of type 3 in **Figure 4.1**. The salient feature here is that there is a fixed point inside an unstable limit cycle inside a stable limit cycle. Corroborating this result, we keep $\phi = 0.04$ fixed and vary I only. That gives us the bifurcation diagram in **Figure 4.3**.

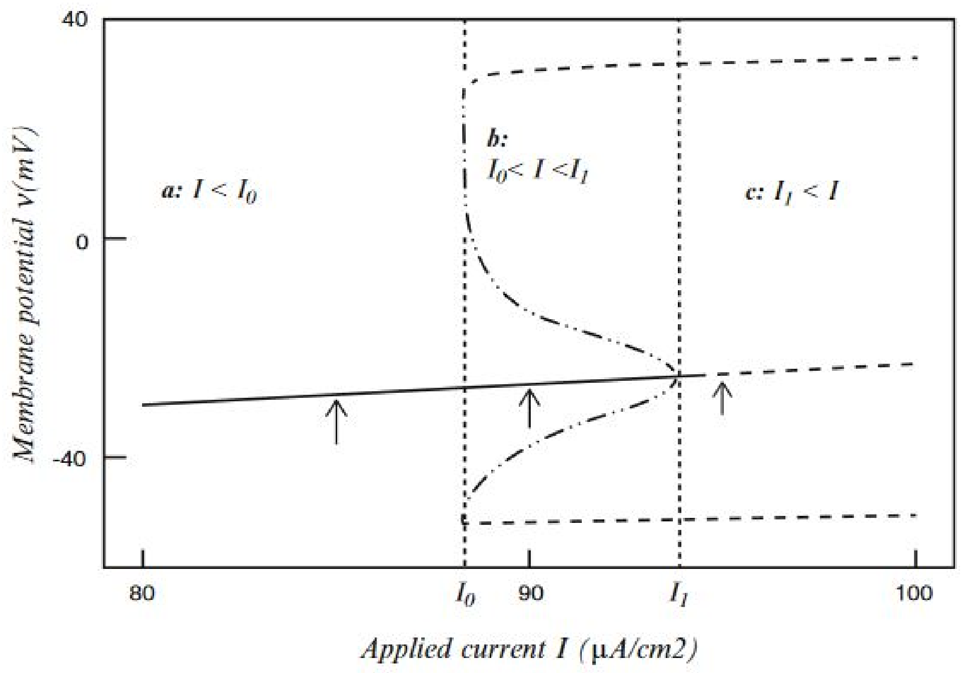

Figure 4.3: *TODO: get better image (maybe plot in python?)*

In the (v, w) phase plane, trajectories closing in on the fixed point represent *quiescent* oscillations. In contrast, trajectories orbiting near the stable limit cycle exhibit *spiking* oscillations. Since this system is bistable, these are the only types of oscillations that can arise. The switching between the quiescent and spiking states describe neuronal behaviour and is of interest to us. Example phase portraits and corresponding $v(t)$ signals of deterministic quiescent and spiking oscillations are given in **Figure 4.4** and **Figure 4.5**, respectively.

These figures can be reproduced by running the `ml` script:

```
python -m scripts.ml
```

To get a deterministic trajectory, set the `stochastic_method` variable in the `scripts/ml.py` file to `None`:

```
stochastic_method = None
```

For a quiescent trajectory, set the initial condition

```
x0 = np.array([-30.0, 0.15])
```

and run the script. Meanwhile, for a spiking trajectory, set the initial condition

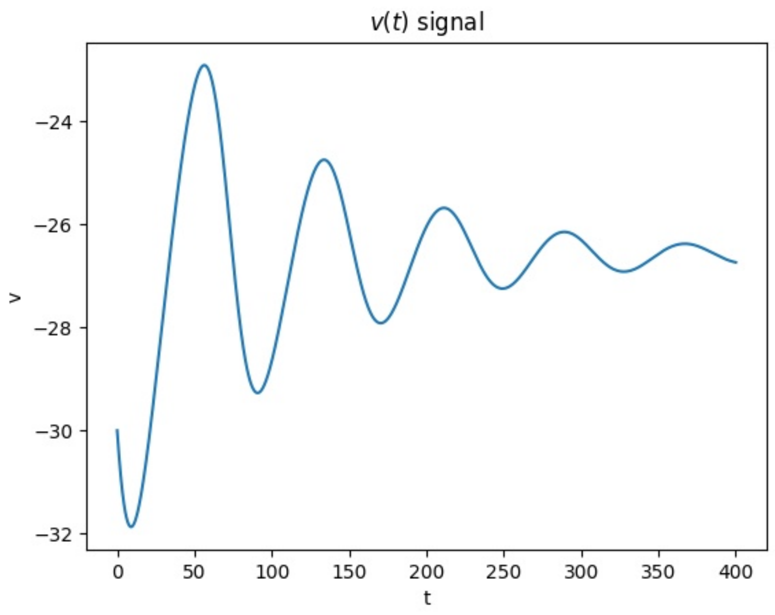

(a)

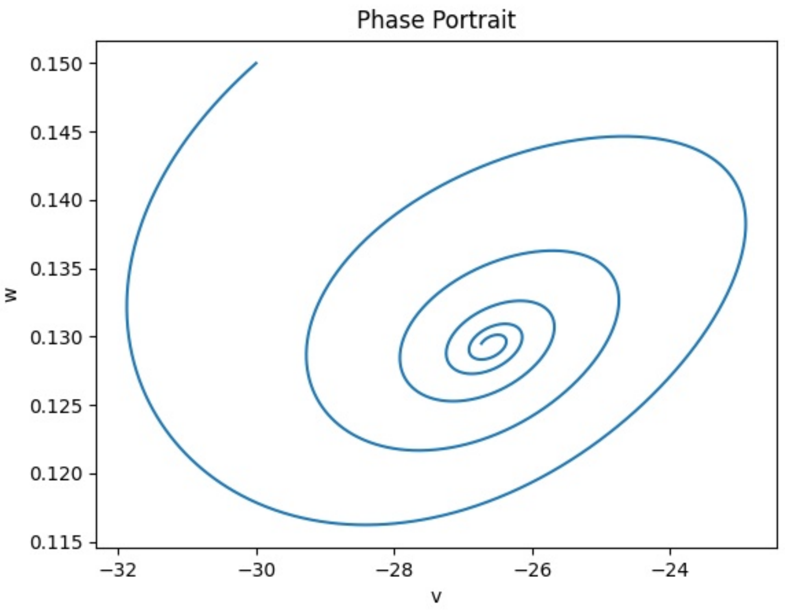

(b)

Figure 4.4: *Quiescent trajectory with initial point* $(-30.0, 0.15)$ *and* $t_{max} = 400$. *As is the case for this report, voltage and time have units of* mV *and* ms*, respectively.*

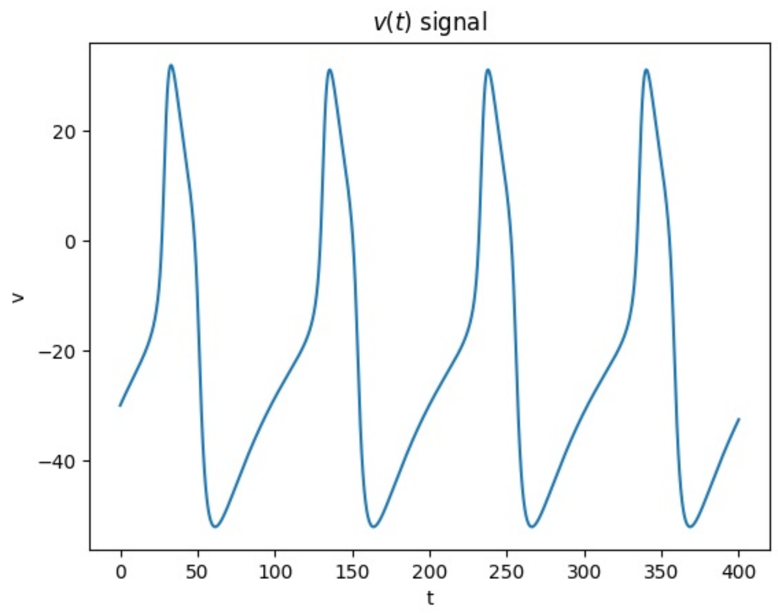

(a)

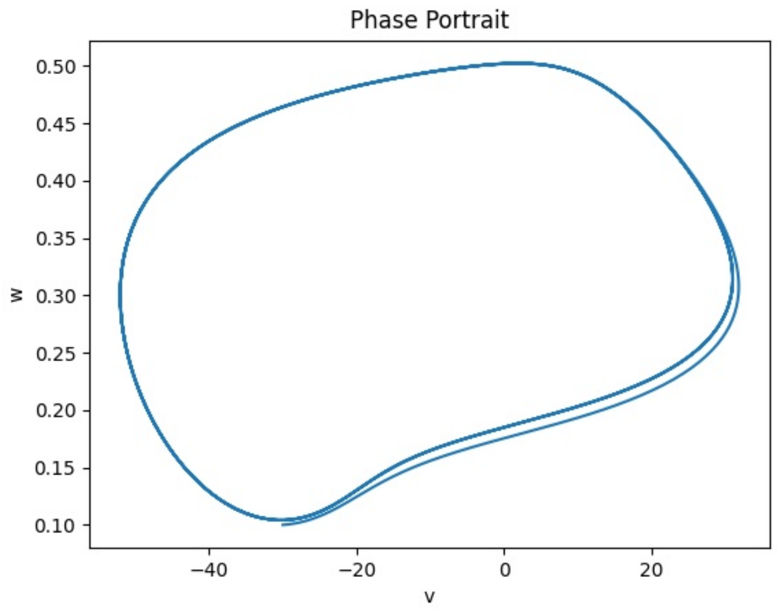

(b)

Figure 4.5: *Spiking trajectory with initial point* $(-30.0, 0.1)$ *and* $t_{max} = 400$.

```
        x0 = np.array([-30.0, 0.1])
```

and run the script.

4.3 Scaling Results

The results in this section were obtained with the use of `MATCONT` [2].

Some potentially interesting scaling results in the Morris-Lecar neuron were obtained. First, along the H_+ curve in the Bautin bifurcation diagram, the fixed point has two imaginary eigenvalues that are conjugates of each other (since the real part goes to zero for Hopf bifurcations). It turns out that this imaginary part ω scales as $\sqrt{\phi}$:

$$\omega \sim \sqrt{\phi} \tag{4.10}$$

This fit is compared to the numerical data in **Figure 4.6**.

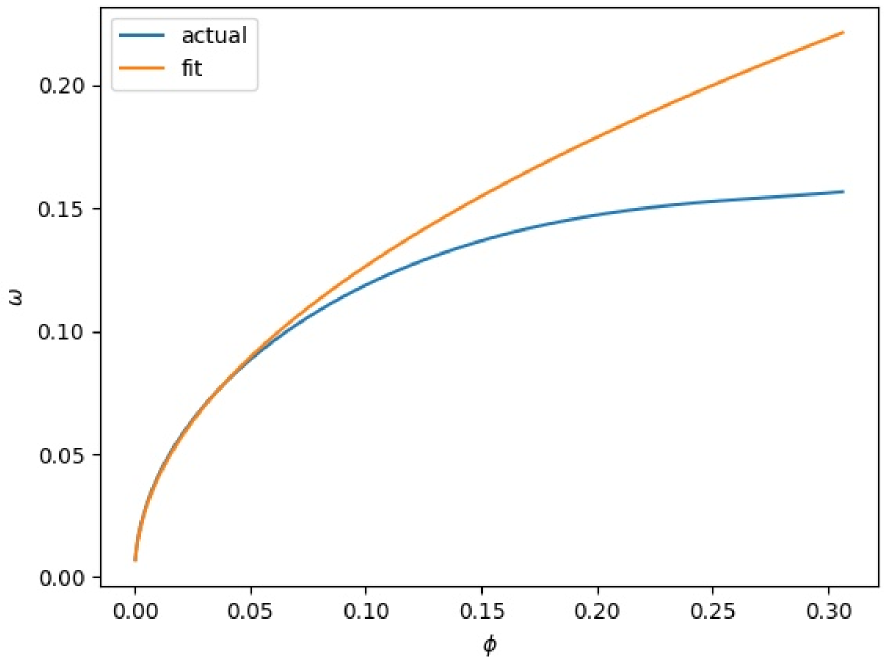

Figure 4.6: *Comparison of fit power law scaling and actual numerical data for $\omega(\phi)$ at small ϕ. The fit obeys the equation $\omega = 0.4\sqrt{\phi}$.*

This agrees with the theoretical result obtained in [1] (in that paper, the authors use ε and λ in place of ϕ and I, respectively).

The scaling between I and ϕ along the H_+ and SNLC curves for small ϕ was also investigated. Along the H_+ curve we have:

$$I \sim \phi \tag{4.11}$$

Along the SNLC curve we get:

$$I \sim \phi^{4/3} \tag{4.12}$$

These fits are compared to numerical data in **Figure 4.7**.

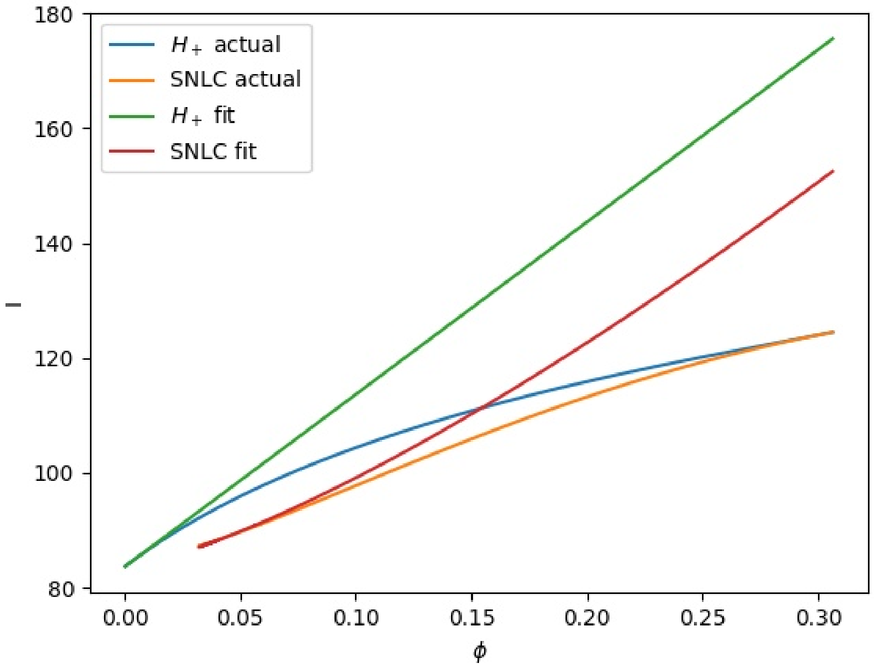

Figure 4.7: *Comparison of fit power law scaling and actual numerical data for $I(\phi)$ at small ϕ along the H_+ and SNLC bifurcation curves. The fits obey the relationships $I = 300\,\phi$ and $I = 333.3\,\phi^{4/3}$ along the H_+ and SNL curves, respectively.*

4.4 Helpful Resources

The book [9] provides an excellent introduction to bifurcation theory. A more advanced book on bifurcation theory is [5]. Meanwhile, the software `MATCONT` [2], which can be run through MATLAB, is really useful for numerical bifurcations. A helpful tutorial guide for `MATCONT` is [7].

5 Stochastics

5.1 Itô Calculus

X_t is a *Wiener process* iff it is a continuous-time stochastic process satisfying the following conditions [6]:

1. **Stationary increments:** If $s \leq t$, $X_t - X_s$ has the same distribution as $X_{t-s} - X_0$.
2. **Independent increments:** If $s \leq t$, $X_t - X_s$ is independent of X_r for all $r \leq s$.
3. **Continuous paths:** X_t is a continuous function of t.

Here, a Wiener process is characterized by three paramters: the initial condition X_0, the drift m, and the variance parameter σ^2. For $s \leq t$, the increment $X_t - X_s$ is distributed as a Gaussian with mean $m(t-s)$ and variance $\sigma^2(t-s)$:

$$X_t - X_s \sim N\left(m(t-s), \sigma^2(t-s)\right) \tag{5.1}$$

The *standard* Wiener process B_t has $B_0 = 0$, $m = 0$, and $\sigma^2 = 1$. We may therefore write

$$dX_t = mdt + \sigma dB_t \tag{5.2}$$

Note that dB_t is distributed as

$$dB_t \sim \sqrt{dt}Z \tag{5.3}$$

where Z is a standard normal random variable. Now in general, if f is a function of X_t, then we may write

$$df(X_t) = g(X_t)dt + h(X_t)dB_t \tag{5.4}$$

for some functions $g(X_t), h(X_t)$ (Itô's lemma gives a more precise result, but we will not utilize it for these purposes).

The n-dimensional standard Wiener process $\mathbf{B_t}$ is simply a vector of n independent standard Wiener processes. Then an n-dimensional dyanmical system $\mathbf{X}$ can be expressed in the form

$$d\mathbf{X} = \mathbf{g}(\mathbf{X})dt + \mathbf{H}(\mathbf{X})\mathbf{dB_t} \tag{5.5}$$

Here $\mathbf{g}$ is a vector while $\mathbf{H}$ is a matrix.

5.2 Stochastic Morris-Lecar

We can model the neuron as having N_K potassium channels (in this project, we are typically on the order of $N_K \sim 1000$), each of which can be fully open or closed. The opening rate (i.e. probability rate of transition from the closed state to the open state) and closing rate for each channel would be $\alpha(v)$ and $\beta(v)$ from (3.5), respectively. Then over a small time increment dt, the probability of a closed channel opening is $\alpha(v)dt$. Likewise, the probability of an open channel closing is $\beta(v)dt$.

Over a time increment of dt, we have

$$dw = w(t+dt) - w(t) \sim \frac{\text{Binom}\left(N_K(1-w), \alpha dt\right) - \text{Binom}\left(N_K w, \beta dt\right)}{N_K} \tag{5.6}$$

Note that $\text{Binom}\left(n, p, =\right) \sum_{j=1}^{n} I_j$, where each I_j is an independent indicator random variable with probability p. By the central limit theorem, when n is large

$$\text{Binom}\left(n, p\right) \sim np + \sqrt{np(1-p)}Z \tag{5.7}$$

where Z is a standard normal random variable. Then (5.6) becomes

$$dw \sim \frac{\left(N_K(1-w)\alpha dt + \sqrt{N_K(1-w)\alpha dt(1-\alpha dt)}Z_1\right) - \left(N_K w\beta dt + \sqrt{N_K w\beta dt(1-\beta dt)}Z_2\right)}{N_K} \tag{5.8}$$

Here Z_1 and Z_2 are independent normal random variables. This is because the closed and open channels are independent (as we assumed all the channels to be independent). Since dt is small, $1 - \alpha dt \approx 1$. So

$$dw \sim \left(\alpha(1-w) - \beta w\right) dt + \frac{1}{\sqrt{N_K}}\sqrt{\alpha(1-w) + \beta w}\sqrt{dt}Z \tag{5.9}$$

As a system of stochastic differential equations, we have

$$\begin{pmatrix} v \\ w \end{pmatrix}' = \begin{pmatrix} f(v,w) \\ g(v,w) \end{pmatrix} dt + \begin{pmatrix} 0 & 0 \\ 0 & h(v,w) \end{pmatrix} \mathbf{dB_t} \tag{5.10}$$

$$f(v,w) = \frac{I - \bar{g}_K w(v - V_K) - \bar{g}_{Ca} m_\infty(v)(v - V_{Ca}) - g_L(v - V_L)}{C} \tag{5.11}$$

$$g(v,w) = \alpha(v)(1-w) - \beta(v)w \tag{5.12}$$

$$h(v,w) = \frac{1}{\sqrt{N_K}}\sqrt{\alpha(v)(1-w) + \beta(v)w} \tag{5.13}$$

Example phase portraits and corresponding $v(t)$ signals of stochastic quiescent and spiking oscillations are given in **Figure 5.1** and **Figure 5.2**. Note that the trajectory in **Figure 5.1** transitions between quiescent and spiking states, as opposed to staying in the quiescent state like its deterministic counterpart. Such transitioning between quiescent and spiking states make the neuronal behaviour interesting and is worthy of closer investigation.

5.3 Euler-Maruyama Method

The Euler-Maruyama method is a generalization of the Euler method to stochastic differential equations of the form (5.5). Here, a small finite time increment dt is chosen.

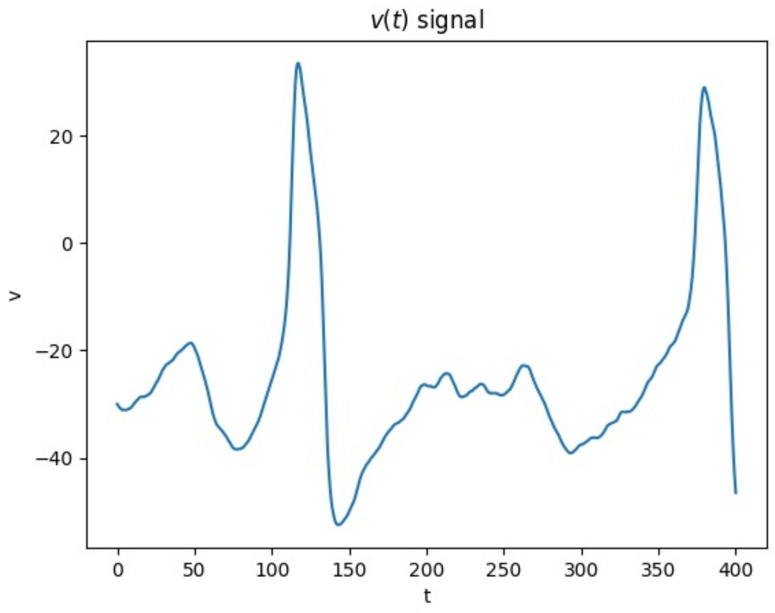

(a)

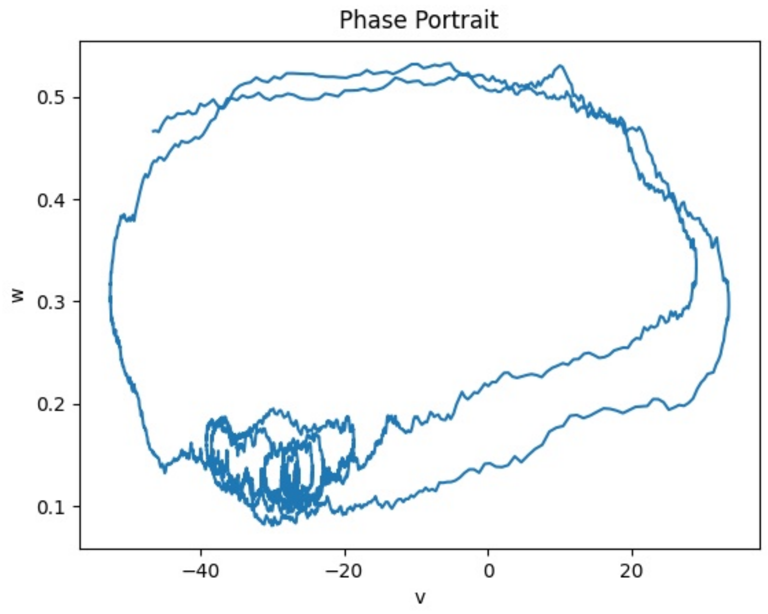

(b)

Figure 5.1: *Stochastic trajectory with initial point* $(-30.0, 0.15)$ *and* $t_{max} = 400$*. Parts of the trajectory are quiescent while other parts are spiking.*

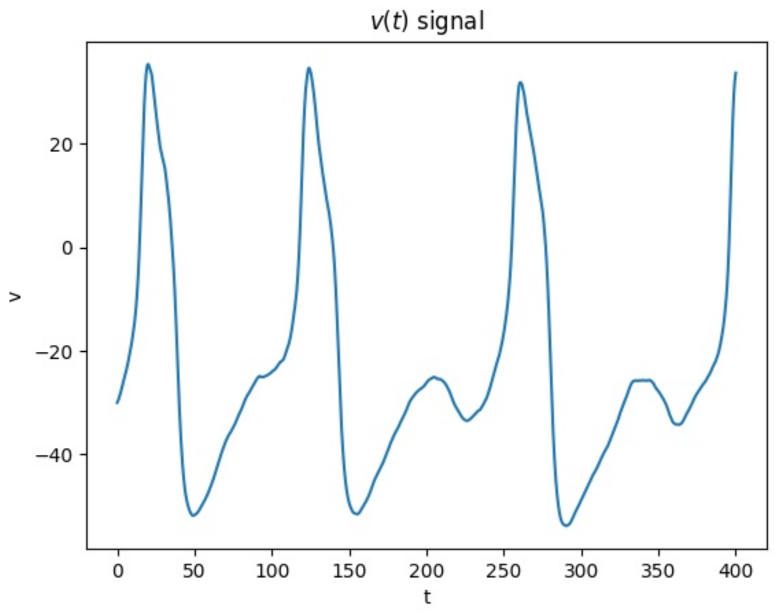

(a)

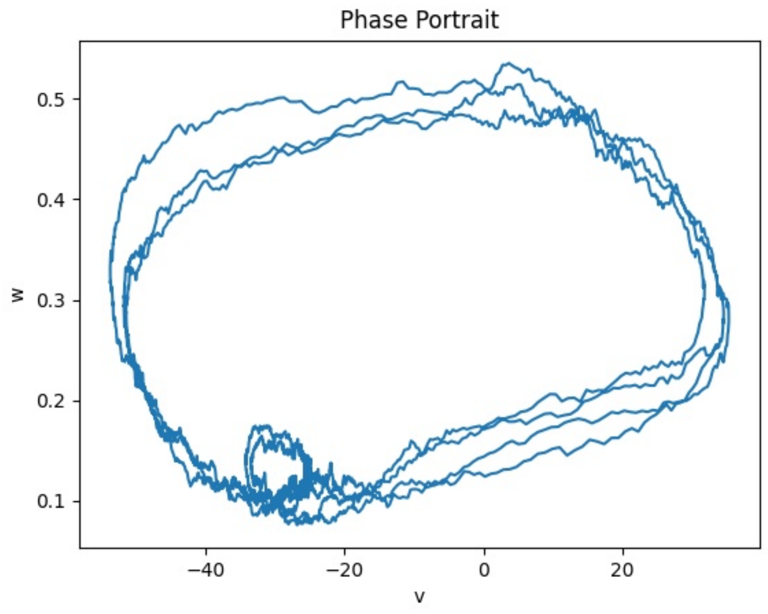

(b)

Figure 5.2: *Stochastic spiking trajectory with initial point* $(-30.0, 0.1)$ *and* $t_{max} = 400$.

Then, starting from an initial condition $\mathbf{X}(0)$, we iteratively compute

$$\mathbf{X}(t+dt) = \mathbf{X}(t) + \mathbf{g}(\mathbf{X})dt + \mathbf{H}(\mathbf{X})\mathbf{Z}\sqrt{dt} \tag{5.14}$$

Here $\mathbf{Z}$ is a randomly generated vector, where each entry is obtained from an independent unit normal distribution. The resulting path $\mathbf{X}(t)$ will be distributed approximately as the true distribution; thus, many trials of the Euler-Maruyama method can be used to obtain statistics for the process (e.g. ISIs, which will be discussed later).

To ease computations, only the second entry of $\mathbf{Z}$ needs to be generated for the 2-dimensional stochastic Morris-Lecar model (since only $\mathbf{H_{22}}$ is nonzero). Furthermore, the random numbers can all be generated at the start rather than at every iteration.

The Euler-Maruyama method is implemented in the project's software. One such script that utilizes this is `scripts/ml.py`. Here a stochastic trajectory of the Morris-Lecar neuron can be simulated using the Euler-Maruyama method. This can be done by first setting the appropriate stochastic method in the file:

```
stochastic_method = 'euler'
```

Then the script can be run in a terminal:

```
python -m scripts.ml
```

The plots in **Figure 5.1** and **Figure 5.2** can be reproduced (up to stochastic noise) by running this script with the Euler-Maruyama method.

5.4 Helpful Resources

The book [6] provides a great introduction to stochastic calculus.

6 Interspike Intervals

One statistic of interest in this project is the ISI distribution. Intuitively, these intervals are the lengths of time between successive spikes in the membrane potential. Adding stochastics to the Morris-Lecar neuron results in a probabilistic distribution of intervals.

6.1 Defining Intervals

6.2 Results

7 Poincare-Like Maps

TODO

8 Alternative Dynamics

8.1 Jacobi Dynamics

Physically, w should be bounded in $[0,1]$. However, the equations described in (5.10)-(5.13) imply a finite (albeit small) possibility of w being outside of $[0,1]$. *In practice*, this issue never really manifests. For theoretical satisfaction, however, we may instead use–for a fixed v–a bounded diffusion process for w.

Following [3], we choose the simplest diffusion process that mimics the system. Arguably, we wish to preserve the dynamic part $g(v,w)$ while having as simple of a variance coefficient $h(v,w)^2$ as possible. The preservation of $g(v,w)$ can be vouched for as it, loosely speaking, determines the "average" behaviour of the system, as well as defining the $N_K \to 0$ limit behaviour. Seeing that $g(v,w)$ is linear in w, we consider Pearson diffusions, where $h(v,w)^2$ is a polynomial of degree at most two. It turns out that the Jacobi diffusion is the only Pearson diffusion bounded in a finite interval. This renders a Jacobi diffusion as the "simplest" bounded diffusion process appropriate for the stochastic Morris-Lecar system.

We follow the discussion [3] on the Jacobi diffusion here. The Jacobi diffusion bounded on $(0,1)$ has the form (for fixed v)

$$dw = -\theta(w-\mu)dt + \gamma\sqrt{2\theta w(1-w)}dB_t \tag{8.1}$$

Equating the dynamic part gets us

$$\theta = \alpha + \beta, \quad \mu = \frac{\alpha}{\alpha+\beta} \tag{8.2}$$

Note that we necessarily have $\alpha(v), \beta(v) \geq 0$ as can be seen from (3.6)-(3.7). The Jacobi diffusion is *ergodic* for

$$\gamma^2 \leq \mu, 1-\mu \tag{8.3}$$

To retain this property, we can rewrite $\gamma = \sigma^*\delta(v)$, where σ^* is a constant that can be fit (to e.g. match $h(v,w)$ at the fixed point) and $\delta(v)$ is a simple function of v. Of course, such a choice of $\sigma^*, \delta(v)$ is not unique since we can rewrite $\sigma^* \mapsto x\sigma^*$, $\delta(v) \mapsto \frac{\delta(v)}{x}$ for any nonzero x. We therefore assert the condition that $\sigma^* \in [0,1]$ and that (8.3) holds for all σ^* in that range. When fitting σ^*, the ergodicity requirement becomes verifying that $\sigma^* \in [0,1]$.

γ^2 is largest when $\sigma^* = 1$, so our task becomes assuring that $\delta(v)^2 \leq \mu, 1-\mu$ i.e.

$$\delta(v)^2 \leq \frac{\alpha(v)}{\alpha(v)+\beta(v)}, \frac{\beta(v)}{\alpha(v)+\beta(v)} \tag{8.4}$$

Naively, we could define

$$\delta(v) = \sqrt{\min\left(\frac{\alpha(v)}{\alpha(v)+\beta(v)}, \frac{\beta(v)}{\alpha(v)+\beta(v)}\right)} \tag{8.5}$$

However, the piecewise definition comes at the cost of differentiability. To make $\delta(v)$ analytically "well-behaved", we instead define $\delta(v)^2$ to be the harmonic sum of $\mu, 1-\mu$ (as is done for e.g. parallel resistors):

$$\delta(v)^2 = \frac{\mu(1-\mu)}{\mu + (1-\mu)} = \frac{\alpha\beta}{\alpha+\beta} \tag{8.6}$$

Thus

$$\gamma = \sigma^* \sqrt{\frac{\alpha\beta}{\alpha+\beta}} \tag{8.7}$$

Equation (8.1) now becomes

$$dw = (\alpha(v)(1-w) - \beta(v)w)dt + \sigma^* \sqrt{2\frac{\alpha(v)\beta(v)}{\alpha(v)+\beta(v)} w(1-w)} dB_t \tag{8.8}$$

The fixed point of the system occurs at approximately $(v_{eq}, w_{eq}) = (-26.6, 0.129)$. Plugging this into (5.13) and the coefficient in front of dB_t in (8.8) gives

$$h(v_{eq}, w_{eq}) = \frac{0.1003}{\sqrt{N_K}} = 0.03365\sigma^* \tag{8.9}$$

That gives us

$$\sigma^* = \frac{2.98}{\sqrt{N_K}} \tag{8.10}$$

Since N_K is on the order of 1000, and certainly larger than 9, we see that typical fits of σ^* are indeed ergodic.

8.2 Linearized Dynamics

Near the fixed point, we can expand (5.10) as a linear model as in [3]. Since the deterministic part is zero to zeroth order, we expand it to first order. In contrast, the stochastic part $h(v, w)$ is nonzero to zeroth order, so we need only expand that to zeroth order. That gets us

$$\begin{pmatrix} v \\ w \end{pmatrix}' \approx \mathbf{M} \begin{pmatrix} v \\ w \end{pmatrix} dt + \begin{pmatrix} 0 \\ \frac{0.1003}{\sqrt{N_K}} dB_t \end{pmatrix} \tag{8.11}$$

Here we used the value of (8.9) for the stochastic part. Meanwhile, $\mathbf{M}$ is the Jacobian matrix of the dynamic part in (5.10):

$$\mathbf{M} = D \begin{pmatrix} f(v, w) \\ g(v, w) \end{pmatrix} \tag{8.12}$$

The linear approximation is valid in a small region near the fixed point. Of course, this region is necessarily within the unstable limit cycle. Numerical experiemnts can provide more clarity into the size of this region. Such a region would be elliptical, however. This is because the coordinates v, w are not symmetrical in the sense that $\mathbf{M}$ does not stretch and shear them uniformly. To remove this complication and simplify the equation, we can define the matrix

$$\mathbf{Q} = \begin{pmatrix} \omega & m_{11} + \lambda \\ 0 & m_{21} \end{pmatrix} \tag{8.13}$$

Then we define

$$\mathbf{A} = \mathbf{Q}^{-1}\mathbf{M}\mathbf{Q} = \begin{pmatrix} -\lambda & \omega \\ -\omega & -\lambda \end{pmatrix} \tag{8.14}$$

$$\tilde{\mathbf{x}} = \mathbf{Q}^{-1} \begin{pmatrix} v \\ w \end{pmatrix} \tag{8.15}$$

$$\mathbf{c} = \mathbf{Q}^{-1} \begin{pmatrix} 0 \\ \frac{0.1003}{\sqrt{N_K}} dB_t \end{pmatrix} \tag{8.16}$$

We then obtain the symmetrized equation

$$d\tilde{\mathbf{x}} = \mathbf{A}\tilde{\mathbf{x}} + \mathbf{c} \tag{8.17}$$

In the transformed space $\tilde{\mathbf{x}}$, it makes sense to talk about circular regions as opposed to elliptical regions in the original coordinate system. Finally, we can further simplify this equation by factoring out rotations. If we define

$$\tilde{\tilde{\mathbf{x}}} = R_{\omega t}\tilde{\mathbf{x}} = \begin{pmatrix} \cos \omega t & -\sin \omega t \\ \sin \omega t & \cos \omega t \end{pmatrix} \tilde{\mathbf{x}} \tag{8.18}$$

Then we obtain the equation

$$d\tilde{\tilde{\mathbf{x}}} = -\lambda\tilde{\tilde{\mathbf{x}}} + R_{\omega t}\mathbf{c} \tag{8.19}$$

8.3 Numerical Comparison

TODO

8.4 Helpful Resources

The article [3] discusses these alternative models as well.

9 Patched Model

10 Next Steps

References

[1] S. M. BAER and T. ERNEUX. Singular hopf bifurcation to relaxation oscillations. *SIAM journal on applied mathematics*, 46(5):721–739, 1986.

[2] A. Dhooge, W. Govaerts, and Yu Kuznetsov. Matcont: A matlab package for numerical bifurcation analysis of odes. *ACM transactions on mathematical software*, 29(2):141–164, 2003.

[3] Susanne Ditlevsen and Priscilla Greenwood. The morris–lecar neuron model embeds a leaky integrate-and-fire model. *Journal of mathematical biology*, 67(2):239–259, 2013;2011;.

[4] Priscilla E. Greenwood, Lawrence M. Ward, SpringerLink (Online service), SpringerLINK ebooks Mathematics, and Statistics. *Stochastic Neuron Models*, volume 1.5. Springer International Publishing, Cham, 1st 2016. edition, 2016.

[5] Yuri A. Kuznetsov, SpringerLINK eBooks English/International Collection (Archive), and SpringerLink (Online service). *Elements of Applied Bifurcation Theory*, volume 112. Springer New York, New York, NY, third;third; edition, 2004;2013;.

[6] Gregory F Lawler. Stochastic calculus: An introduction with applications. *American Mathematical Society*, 2010.

[7] Hil Meijer. Matcont tutorial: ode gui version, 2016.

[8] C. Morris and H. Lecar. Voltage oscillations in the barnacle giant muscle fiber. *Biophysical journal*, 35(1):193–213, 1981.

[9] Steven H Strogatz. *Nonlinear dynamics and chaos with student solutions manual: With applications to physics, biology, chemistry, and engineering.* CRC press, 2018.

[10] David H. Terman and G. B. Ermentrout. *Foundations of mathematical neuroscience*, volume 35. Springer, 2010.